The role of octahedral cations in pyroxenoid crystal chemistry. I. Bustamite, wollastonite, and the pectolite–schizolite–serandite series

YOSHIKAZU OHASHI[1] AND LARRY W. FINGER

Geophysical Laboratory, Carnegie Institution of Washington
Washington, D. C. 20008

Abstract

Crystal structures and cation occupancies have been refined using single-crystal X-ray diffraction data for natural specimens of (1) manganoan, intermediate, and calcian bustamites; (2) ferroan and manganoan wollastonites; and (3) serandite and manganoan pectolites (schizolite). Although the silicate chains of three-tetrahedral repeat are similar in these minerals, the differences in cation arrangements in the octahedral layers result in three structures with distinct stacking schemes of tetrahedral and octahedral layers. The unchanged occupancies in the $M3$ and $M4$ sites of bustamite, $M3$ site of wollastonite, and Na site of pectolite are important for determination of the structure types, whereas the stepwise substitutions in $M1$ and $M2$ explain the observed compositional variations in bustamite and pectolite.

Introduction

Silicate minerals are usually classified according to the manner in which the silicate tetrahedra are linked together (*e.g.* Zoltai, 1960; Bragg *et al.*, 1965; Liebau, 1972). This scheme of classification is, unfortunately, sometimes overemphasized to the extent that the roles of other cations are regarded as of secondary importance. One exception is Belov (1961), who emphasized the role of large cations.

In a short note on the amphibole structure, Thompson (1970) proposed his model of *biopyriboles* (*bio*tite + *pyro*xene + amph*ibole*). Rather than emphasizing a sheet or chain nature of the tetrahedral arrangement, he considers these minerals as made up of (a) tabular units parallel to (010) and also (b) alternating octahedral and tetrahedral layers parallel to (100) of pyroxene and amphibole or (001) of mica. Thus, in his model the octahedral cations have an importance equal to that of the tetrahedra. A recent discovery by Veblen and Burnham (1975, 1976) of minerals intermediate between chain and sheet silicates indicates the practical significance of the biopyribole model.

Geometrical relationships between octahedral and tetrahedral layers have been extensively discussed for

pyroxene (Papike *et al.*, 1973) and for amphiboles (Papike and Ross, 1970). Pyroxenoids, which also have single tetrahedral chains, but with a unit repeat longer than in pyroxenes, can also be regarded as composed of alternating octahedral and tetrahedral layers (Prewitt and Peacor, 1964).

In a series of papers on pyroxenoid crystal chemistry, the role of octahedral cations in pyroxenoids in relation to (1) the repeat distance of the tetrahedral chains and (2) the stacking scheme of the octahedral and tetrahedral layers will be examined. In this first paper the results of cation-occupancy refinements in wollastonite, bustamite, and the pectolite–schizolite–serandite series are discussed in an effort to analyze crystal structural factors that might control the limits of cation substitutions in the octahedral sites or the compositional limits observed in natural pyroxenoid minerals.

The composition of wollastonite is commonly close to the ideal composition $CaSiO_3$, and other components such as $MnSiO_3$ or $FeSiO_3$ rarely exceed a few mole percent. In contrast, bustamite, which is closely related to the wollastonite structure, has a very wide compositional range, with a $CaSiO_3$ content ranging from approximately 30 mole percent to more than 80 mole percent (Mason, 1973, 1975; Hodgson, 1975; Shimazaki and Yamanaka, 1973; Matsueda, 1973). Both wollastonite and bustamite are structurally characterized by single silicate chains

---

with a repeat of three tetrahedra. Hydrous counterparts for wollastonite and bustamite are pectolite (end member: $NaCa_2HSi_3O_9$) and serandite (end member: $NaMn_2HSi_3O_9$) with complete solid solution between the end members (Schaller, 1955). A mineral name, schizolite, is used for manganoan pectolite.

These three mineral groups—wollastonite, bustamite, and the pectolite–schizolite–serandite series—have similar silicate tetrahedral chains yet differ greatly in the extent of substitution of octahedral cations.

Previous work

Crystal structure

Wollastonite, bustamite, and pectolite, mainly owing to their similarity in morphology, were long regarded as minerals that belonged to the same family. Proposed structures of wollastonite (Mamedov and Belov, 1956) and pectolite (Buerger, 1956), however, were not the same. This difference led Buerger and his coworkers to more detailed analyses of the structures of the minerals. On the basis of structural refinements, Buerger and Prewitt (1961) concluded that both proposed structures were correct. Prewitt and Buerger (1963) described the differences and similarities between these two structures. The pectolite structure was further refined by Prewitt (1967). Schizolite, manganoan pectolite, is isostructural with pectolite (Liebau, 1958).

The structure of bustamite, once described incorrectly as Mn-rich wollastonite (Sundius, 1931; Schaller, 1955), has been shown to be distinct from wollastonite (Peacor and Buerger, 1962). These two minerals differ in the arrangement of the tetrahedral layers relative to the octahedral layers (Peacor and Prewitt, 1963).

Chemical compositions

The distinction between wollastonite and Ca-rich bustamite was not clearly stated in the mineralogical literature until the early 1970's. From phase-equilibrium and spectroscopic studies, Rutstein (1971) and Rutstein and White (1971) suggested the existence of immiscibility between the two minerals. Matsueda (1973, 1974) described "iron-wollastonite" of the composition $(Ca_{0.82}Fe_{0.14}Mn_{0.02}Mg_{0.01})SiO_3$ from the Sampo Mine, Japan, which shows properties more like those of bustamite than those of wollastonite in infrared, Mössbauer, and powder X-ray diffraction experiments. Similar "iron-wollastonite," which was

later confirmed to have the bustamite structure, was also reported from Kagata Mine, Japan, by Shimazaki and Yamanaka (1973) as a phase distinct from ordinary wollastonite. Rapoport and Burnham (1972, 1973) suggested that the maximum Ca limit of the bustamite structure would occur at the $Ca_{5/6}Fe_{1/6}SiO_3$ composition.

Compositional limits of wollastonite and bustamite have recently been discussed by Mason (1975), who examined several natural specimens of the minerals. The most important occurrence is coexisting wollastonite and bustamite in a specimen from Franklin, New Jersey. The grain size is, however, too small for the single-crystal diffraction method (see Mason, 1975, Fig. 1 of photomicrograph). Mason (1975) also reported a manganoan wollastonite with approximately 10 mole percent $MnSiO_3$ from Gjellebekk, Norway, which was kindly donated for further X-ray study. Although the Gjellebekk sample is large enough for single-crystal study, precession photographs of the sample show a bustamite-like (not wollastonite-like) pattern. There are diffuse streaks, however, radiating from the ordinary spots. An electron microprobe analysis of the same grain used for the precession study yielded 9–11 mole percent $MnSiO_3$, confirming the original chemical analysis of the sample.

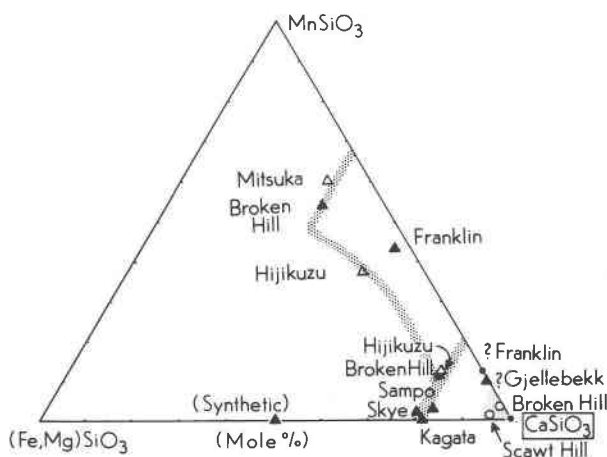The wollastonite field extends from the $CaSiO_3$

Fig. 1. Compositional variation of bustamite (triangles) and wollastonite (circles). Open symbols indicate mineral samples used in this study. Sources of data: Broken Hill (Hodgson, 1975; Mason, 1973, 1975); Sampo (Matsueda, 1973); Kagata (Shimazaki and Yamanaka, 1973); Skye and synthetic bustamites (Rapoport and Burnham, 1973); and Franklin bustamite (Peacor and Buerger, 1962). For discussion of wollastonite samples from Franklin and Gjellebekk, see text (section on "Chemical compositions").

corner to 10 mole percent $MnSiO_3$ and 5 mole percent $FeSiO_3$ (Mason, 1973, Fig. 3). For high-manganese compositions, however, crystal growth of a single phase of wollastonite seems to become extremely difficult. The Gjellebekk sample and probably the Franklin sample could contain complicated microstructures such as stacking disorders with presumably inhomogeneous distributions of Mn.

Cation occupancies

In their original report on determination of the bustamite structure, Peacor and Buerger (1962), using peak-height analysis of difference Fourier maps and interatomic distances, suggested that $M2$ and $M4$ are occupied by Ca and $M3$ is occupied by Mn. Their bustamite sample with 54 mole percent $CaSiO_3$ has a slight excess of Ca that was assigned to $M1$, which is mostly Mn. Thus, the $M1$ site was recognized as a multiple-occupancy site when the structure was first solved.

Rapoport and Burnham (1972, 1973) have con-firmed this general cation-ordering scheme for intermediate compositions in an iron analogue, ferrobustamite ($Ca_{0.5}Fe_{0.5}SiO_3$), synthesized at 1108°C. From the least-squares refinement of cation occupancies they have obtained Ca occupanices of 23, 78, 7, and 92 percent, respectively, in the $M1$, $M2$, $M3$, and $M4$ sites in bustamite. For $M3$ and $M4$, the ordering of Ca and Fe is almost complete, but $M1$ and $M2$ are more disordered, probably reflecting the relatively high temperature at which the crystal was synthesized.

The second crystal Rapoport and Burnham (1972, 1973) investigated is a very Ca-rich ferrobustamite from Skye, Scotland. The composition of this sample is critically important in discussions of cation ordering, especially with relation to the stability of the bustamite and wollastonite structures. Although a twinning problem prevented a meaningful occupancy refinement, Rapoport and Burnham concluded from bond distances that Fe is concentrated primarily in $M(3)$. They have further pointed out that a compo-

Table 1. Description of pyroxenoid specimens

| Sample* | Bustamite | | |
	Mn–BS	BS	Ca–BS
Locality Latitude and longitude	Mitsuka, Gifu, Japan 35°30'N 136°30'E	Hijikuzu, Iwate, Japan 39°45'N 141°45'E	
Geological setting	Mn-ore lens aside dolomite marble	Bedded Mn-ore deposit in chart hornfels	
Reference to mineralogy			Nambu et al (1970)
Octahedral cations** Ca	0.314	0.500	0.783
Mn	0.600	0.370	0.122
Fe	0.043	0.120	0.075
Mg	0.043	0.009	0.020

| Sample* | Wollastonite | | Pectolite-serandite series | |
	Mn–WO	Fe–WO	SRN	SCH
Locality	Broken Hill New South Wales Australia	Scawt Hill Antrim Co. Ireland	Rouma, Island of Los, Guinea	Kangerdluarsuk Julianehaab Greenland
Latitude and longitude	32° S 141°30'E	54°45'N 5°45'W	9°30'N 13°45'W	60°45'N 46° W
Geological setting	Pb-Ag-Zn hypo-thermal deposit	Dolerite contact zone	Nepheline-syenite	Sodalite-syenite pegmatite
Reference to mineralogy	Hodgson (1975)	Tilley (1937)	Lacroix (1931) Schaller (1955)	Bφggild (1903) Schaller (1955)
Octahedral cations** Ca	0.961	0.949	0.162	0.613
Mn	0.034	0.005	0.805	0.319
Fe	0.005	0.036	0.032	0.068
Mg	0.000	0.010	0.000	0.000

* Original specimen numbers: Mn-BS (National Science Museum, Japan. Domestic Collection #20159)
   BS   (Nambu, X-6410)   Fe-WO (U.S. National Museum #10618)
   Ca-BS (Nambu, X-4487)   SRN   (U.S. National Museum #96515)
   Mn-WO (Hodgson, #1544)   SCH   (Harvard University Museum #84967)
** Normalized to Ca+Mn+Fe+Mg=1

Table 2. Electron microprobe analyses of pyroxenoids

Sample	Mn-Bs	BS	Ca-BS	Mn-WO	Fe-WO	SRN	SCH
			Oxides wt. %				
SiO_2	48.0	48.9	50.5	50.6	50.6	50.2	51.7
FeO*	2.4	7.0	4.4	0.3	2.3	1.3	2.8
MnO	33.9	21.3	7.2	2.1	0.3	32.0	12.8
MgO	1.4	1.4	0.6	0.0	0.4	0.0	0.0
CaO	14.0	22.7	36.4	45.8	46.2	5.1	19.5
Na_2O	--	--	--	--	--	8.6	9.6
Total	99.7	100.2	99.1	98.8	99.8	97.2**	96.4**
		Cations based on 9 oxygens†				on 17 oxygens††	
Si	3.00	3.00	3.00	2.99	2.97	5.99	5.99
Fe	0.13	0.36	0.22	0.02	0.11	0.13	0.27
Mn	1.79	1.11	0.36	0.10	0.02	3.23	1.26
Mg	0.13	0.03	0.06	0.00	0.03	0.00	0.00
Ca	0.94	1.49	2.33	2.90	2.90	0.65	2.42
Na	--	--	--	--	--	1.98	2.15
Total	5.99	5.99	5.97	6.01	6.03	11.99	12.08

* All Fe as FeO
** Excluding H_2O
† For idealized formula $M_3Si_3O_9$
†† For idealized formula $2M_2NaHSi_3O_9$ or $M_4Na_2Si_6O_{17}\cdot H_2O$

Table 3. Unit cell parameters of pyroxenoids*

Sample	Mn-BS	BS	Ca-BS
Space group**	$I\bar{1}$	$I\bar{1}$	$I\bar{1}$
a, Å	9.807(4)	9.864(3)	9.994(3)
b	10.680(4)	10.790(5)	10.946(3)
c	7.091(2)	7.139(3)	7.231(3)
α, deg.	99.58(2)	99.53(4)	99.30(3)
β	99.99(3)	99.71(3)	100.56(3)
γ	83.79(3)	83.83(3)	83.29(2)
Unit cell volume†, Å³	718.8(4)	736.1(5)	764.3(4)

Sample	Mn-WO	Fe-WO	SRN	SCH
Space group**	$C\bar{1}$	$C\bar{1}$	$C\bar{1}$	$C\bar{1}$
a	10.121(2)	10.104(1)	9.909(9)	10.059(4)
b	11.070(1)	11.054(1)	10.667(9)	10.880(8)
c	7.312(1)	7.305(1)	6.913(4)	6.978(6)
α	99.51(1)	99.53(1)	99.10(6)	98.84(7)
β	100.51(1)	100.56(1)	100.51(6)	100.58(5)
γ	83.43(1)	83.44(1)	82.49(7)	82.64(5)
Unit cell volume†, Å³	791.5(2)	788.0(1)	705.5(9)	737.9(9)

* Obtained from least-squares refinement of twelve reflections centered on a four-circle diffractometer. Figures in parentheses represent one standard deviation in terms of the least units cited.

** Cell transformation matrices are [-1,-½,-½ / -1,-½,½ / 0,1,0] from the conventional $A\bar{1}$ cell to $I\bar{1}$ cell for bustamite and [1,0,1 / 1,0,-1 / 0,1,0] from $P\bar{1}$ to $C\bar{1}$ cells for wollastonite and pectolite-serandite.

† Contains 4 formula units of $M_3Si_3O_9$ or $M_2NaHSi_3O_9$.

sition where Ca completely fills $M1$, $M2$, and $M4$ and Fe remains exclusively in $M3$ would be $Ca_{5/6}Fe_{1/6}SiO_3$.

Recently Yamanaka, Sadanaga, and Takéuchi (Y. Takéuchi, personal communication, 1976) have shown by direct-occupancy refinement of X-ray diffraction data that iron atoms are concentrated in the $M3$ site for a Ca-rich ferrobustamite previously described by Shimazaki and Yamanaka (1973).

For the pectolite–schizolite–serandite series, Takéuchi *et al.* (1976b) have reported that Ca is concentrated in $M1$ for a composition $Mn_{1.88}Ca_{0.17}Mg_{0.01}NaHSi_3O_9$.

Experimental

Mineral specimens

Two samples of wollastonite, three of bustamite, and two of the pectolite–schizolite–serandite series (Table 1) were selected for single-crystal X-ray studies. These mineral specimens, in combination with specimens used in other work, represent the range of chemical compositions of wollastonite and bustamite (Fig. 1). The results of electron microprobe analyses of these samples are given in Table 2.

Unit-cell setting

In the conventional setting of the unit cell for the minerals, the two well-developed cleavages are chosen as (100) and (001), with the b axis parallel to the intersection of the cleavage planes. This setting,

however, is not suitable for a structural comparison of pyroxenes and pyroxenoids. The new setting used in this study is analogous to that proposed by Narita (1973; quoted by Morimoto, 1974) and Koto *et al.* (1976).

In the new setting, the layers of octahedra and tetrahedra are, as in pyroxenes, parallel to the b–c plane, and the c axis is the tetrahedral chain direction. Thus the a axis becomes, as in pyroxenes, a direction along which the octahedral and tetrahedral layers are alternately stacked together. The new unit

Table 4. Crystal structure refinement data of pyroxenoids

	Mn-Bs	BS	Ca-BS	Mn-WO	Fe-WO	SRN	SCH
Size of crystal (mm)	0.34x 0.14x 0.14	0.26x 0.07x 0.07	0.42x 0.26x 0.19	0.30x 0.08x 0.06	0.31x 0.08x 0.07	0.37x 0.14x 0.07	0.41x 0.10x 0.07
μ^*,cm⁻¹	46.7	43.0	33.1	25.2	25.7	37.5	27.3
t**,%	51-60	71-82	51-66	81-88	81-85	58-77	76-83
number of reflections	1810	1777	2054	1921	1883	1490	1364
R^+,%	5.2	3.6	4.9	3.5	3.9	6.1	3.6
R(wtd)	5.6	3.7	5.9	3.5	4.1	7.1	4.1

* Linear absorption coefficient for MoKα
** Range of transmission factor
†Residual factors: $R = \Sigma||F_o|-|F_c||/\Sigma|F_o|$
$R(wtd) = [\Sigma w(|F_o|-|F_c|)^2/\Sigma w|F_o|^2]^{1/2}$

OHASHI AND FINGER: PYROXENOID CRYSTAL CHEMISTRY

Table 5. Atomic positional parameters* and isotropic temperature factors of pyroxenoids

Site**		Mn-BS	BS	Ca-BS	Site**		Mn-WO	Fe-WO	Site**		SRN	SCH
M1 (M1,Mn1)	x	0.0241	0.0245	0.0222	M1 (Ca1)	x	0.0208	0.0212	M1 (Ca1)	x	0.0052	0.0026
	y	0.7713	0.7721	0.7771		y	0.7807	0.7800		y	0.6431	0.6485
	z	0.8227	0.8257	0.8179		z	0.0772	0.0772		z	0.9062	0.9063
M2 (M2,Ca1)	x	0.0225	0.0231	0.0247	M2 (Ca2)	x	0.0171	0.0180	M2 (Ca2)	x	0.0082	0.0068
	y	0.7753	0.7783	0.7766		y	0.7806	0.7803		y	0.6416	0.6418
	z	0.3387	0.3410	0.3333		z	0.5709	0.5712		z	0.4158	0.4152
M3 (M3,Mn1)		inversion at (0½½)			M3 (Ca3)	x	0.0144	0.0137	A (Na)	X	0.0462	0.0480
						y	0.4885	0.4889		y	0.8977	0.8965
M4 (M4,Ca2)		inversion at (0½0)				z	0.2504	0.2504		z	0.2473	0.2543
Si1 (Si2)	x	0.2195	0.2226	0.2267	Si1 (Si1)	x	0.2265	0.2265	Si1 (Si1)	x	0.2216	0.2223
	y	0.9565	0.9566	0.9640		y	0.9583	0.9585		y	0.0616	0.0583
	z	0.6435	0.6473	0.6395		z	0.8877	0.8876		z	0.0963	0.0935
Si2 (Si1)	x	0.2223	0.2235	0.2296	Si2 (Si2)	x	0.2267	0.2266	Si2 (Si2)	x	0.2216	0.2221
	y	0.9517	0.9534	0.9573		y	0.9577	0.9576		y	0.0721	0.0708
	z	0.1967	0.1978	0.1983		z	0.4537	0.4540		z	0.5456	0.5403
Si3 (Si3)	x	0.2184	0.2201	0.2209	Si3 (Si3)	x	0.2264	0.2260	Si3 (Si3)	x	0.2017	0.2029
	y	0.1764	0.1757	0.1755		y	0.1707	0.1711		y	0.8446	0.8462
	z	0.9778	0.9801	0.9727		z	0.2236	0.2237		z	0.7597	0.7543
OA1 (O4)	x	0.1200	0.1178	0.1169	OA1 (O3)	x	0.1163	0.1164	OA1 (O5)	x	0.1157	0.1168
	y	0.5802	0.5803	0.5747		y	0.5797	0.5786		y	0.4464	0.4446
	z	0.7766	0.7757	0.7748		z	0.0381	0.0381		z	0.8901	0.8847
OA2 (O3)	x	0.1141	0.1139	0.1109	OA2 (O4)	x	0.1169	0.1168	OA2 (O6)	x	0.1132	0.1160
	y	0.5767	0.5730	0.5733		y	0.5814	0.5807		y	0.4406	0.4415
	z	0.3174	0.3170	0.3200		z	0.5611	0.5612		z	0.3969	0.4036
OA3 (O1)	x	0.1171	0.1164	0.1177	OA3 (O1)	x	0.1149	0.1149	OA3 (O2)	x	0.1346	0.1362
	y	0.3137	0.3135	0.3132		y	0.3141	0.3142		y	0.6892	0.6905
	z	0.4776	0.4744	0.4804		z	0.7307	0.7305		z	0.2133	0.2216
OB1 (O6)	x	0.1106	0.1133	0.1192	OB1 (O5)	x	0.1239	0.1248	OB1 (O3)	x	0.1336	0.1359
	y	0.8568	0.8587	0.8659		y	0.8584	0.8577		y	0.1831	0.1734
	z	0.6399	0.6491	0.6264		z	0.8745	0.8750		z	0.0016	-0.0088
OB2 (O5)	x	0.1297	0.1328	0.1353	OB2 (O6)	x	0.1230	0.1239	OB2 (O4)	x	0.1430	0.1473
	y	0.8379	0.8402	0.8483		y	0.8577	0.8567		y	0.1984	0.1954
	z	0.1026	0.1010	0.1135		z	0.3669	0.3657		z	0.6516	0.6472
OB3 (O2)	x	0.1085	0.1095	0.1084	OB3 (O2)	x	0.1152	0.1147	OB3 (O1)	x	0.1113	0.1112
	y	0.2977	0.2961	0.2925		y	0.2864	0.2874		y	0.7273	0.7335
	z	0.9846	0.9849	0.9772		z	0.2267	0.2271		z	0.7011	0.6957
OC1 (O9)	x	0.2111	0.2105	0.2280	OC1 (O9)	x	0.2211	0.2201	OC1 (O9)	x	0.1725	0.1725
	y	0.9799	0.9787	0.9927		y	0.9963	0.9955		y	0.0657	0.0634
	z	0.4241	0.4259	0.4257		z	0.6785	0.6780		z	0.3090	0.3039
OC2 (O7)	x	0.1678	0.1687	0.1747	OC2 (O8)	x	0.1820	0.1811	OC2 (O8)	x	0.1581	0.1594
	y	0.0876	0.0887	0.0880		y	0.0886	0.0887		y	0.9474	0.9498
	z	0.1206	0.1221	0.1141		z	0.3704	0.3703		z	0.5959	0.5962
OC3 (O8)	x	0.1738	0.1787	0.1787	OC3 (O7)	x	0.1827	0.1823	OC3 (O7)	x	0.1623	0.1703
	y	0.0974	0.0966	0.0988		y	0.0907	0.0912		y	0.9318	0.9270
	z	0.7575	0.7605	0.7560		z	0.0121	0.0119		z	0.9676	0.9664

* Based on the I$\bar{1}$-cell (bustamite) and the C$\bar{1}$-cell (wollastonite and pectolite) with the origin at the inversion center between two tetrahedral triplets across the octahedral layer. Atoms of which coordinates are given in this table correspond to positions labeled in Fig. 3. Coordinates (X,Y,Z) for A-cell (bustamite) and P-cell (wollastonite and pectolite) are transformed to (x,y,z) as follows: x=-½X-Z, y=-½X+Z, z=-½X+Y (bustamite), x=½X+½Z, y=½X-½Z, z=Y+½ (wollastonite) and x=½X+½Z, y=½X-½Z+½, z=Y+½ (pectolite).

** Site names in parentheses are those previously used by Peacor and Buerger (1962), Prewitt and Buerger (1963), Prewitt and Peacor (1964), Rapoport and Burnham (1973), and Takéuchi et al., (1976b) for each mineral.

Table 5, continued

Isotropic temperature factors ($\mathring{A}^2$)

	Mn-BS	BS	Ca-BS	Mn-WO	Fe-WO	SRN	SCH		Mn-BS	BS	Ca-BS	Mn-WO	Fe-WO	SRN	SCH
M1	0.96	0.67	0.64	0.58	0.71	0.80	0.60	OB1	1.84	1.18	1.19	0.81	1.05	1.06	0.89
M2	0.93	0.72	0.71	0.58	0.73	0.86	0.70	OB2	1.67	1.09	0.99	0.88	1.13	0.93	1.15
M3	0.73	0.55	0.64	0.54	0.67	1.58	1.52	OB3	0.78	0.72	0.76	0.56	0.67	0.99	1.02
M4	0.74	0.65	0.64												
								OC1	2.45	1.46	1.26	1.02	1.29	0.88	0.90
Si1	0.54	0.48	0.51	0.42	0.53	0.63	0.63	OC2	0.99	0.81	0.81	0.70	0.85	0.92	0.93
Si2	0.53	0.50	0.50	0.44	0.54	0.64	0.69	OC3	0.97	0.80	0.83	0.73	0.84	0.99	1.02
Si3	0.52	0.48	0.51	0.42	0.52	0.64	0.67								

	Mn-BS	BS	Ca-BS	Mn-WO	Fe-WO	SRN	SCH
OA1	1.12	0.77	0.86	0.76	1.00	0.90	0.94
OA2	1.21	0.84	0.77	0.76	0.98	0.95	1.06
OA3	0.82	0.75	0.72	0.68	0.81	0.89	0.96

Representative standard errors

	M	A	Si	O
x	0.0001	0.0004	0.0001	0.0004
y	0.0001	0.0004	0.0001	0.0004
z	0.0001	0.0004	0.0002	0.0005
B	0.01-0.03	0.03-0.05	0.01-0.02	0.04-0.07

cell is a multiple cell; a body-centered cell for bustamite and a *C*-centered cell for wollastonite and pectolite–serandite.

Unit-cell data with this new setting are given in Table 3. The cell transformation matrices are also given in a footnote to Table 3. (The cell for bustamite is different from that used by Koto *et al.*, 1976.)

Data collection and refinements

The X-ray intensities of all the pyroxenoid crystals used in this study were measured on the automated four-circle diffractometer, employing an ω-2θ variable scanning-rate technique (Finger *et al.*, 1973) and Nb-filtered Mo$K\alpha$ radiation. Integrated intensities were corrected for Lorentz and polarization effects, and absorption corrections were computed by numerical integration (Burnham, 1966).

The atomic coordinates of bustamite reported by Rapoport and Burnham (1973), those of wollastonite given by Buerger and Prewitt (1961), and those of pectolite given by Prewitt (1967) were taken as initial values for subsequent least-squares refinements using computer program RFINE2 (Finger and Prince, 1975). Atomic scattering factors for the fully ionized state (except O⁻) and dispersion corrections are from Cromer and Mann (1968) and Cromer (1965), respectively. Refinement data are summarized in Table 4, and the refined atomic coordinates and isotropic temperature factors are given in Table 5.

Results

Cation occupancies

The occupancies in the octahedral sites have been refined using a linear-combination model of Ca–Mn or Ca–Fe with the constraint of bulk composition

(Finger, 1969). Because the atomic scattering curves for X-rays are very similar for Fe^{2+} (24 electrons) and Mn^{2+} (23 electrons), these two elements were grouped together in occupancy refinements. A small amount of Mg^{2+} (10 electrons) that is ignored in the refinements, however, has the effect of increasing the apparent occupancy of Ca^{2+} (18 electrons).

The refined occupancies (Table 6) show that *M*3 and *M*4 in bustamite can be regarded as essentially invariant—*M*3 is the site for smaller cations such as Mn or Fe, whereas *M*4 is the site for Ca. Much of the apparent Ca occupancy in *M*3 of bustamite would probably be attributed to the presence of minor Mg, because the *M*3 octahedron, as discussed below, is the smallest and would be suitable for the Mg ions. Although $MgSiO_3$ is a minor component in the bulk compositions, the maximum Mg occupancy in *M*3 can theoretically be, for example, $0.043 \times 3 \times 2 =$

Table 6. Cation occupancies* in pyroxenoids

Site	Equi-point fraction	Mn–BS Ca	Mn–BS Mn	BS Ca	BS Mn	Ca–BS Ca	Ca–BS Mn
M1	1.0	0.08	0.92(1)	0.13	0.87(1)	0.93	0.07(1)
M2	1.0	0.49	0.51(1)	0.95	0.05(1)	0.95	0.05(1)
M3	0.5	0.19	0.81(2)	-0.05	1.05(1)	0.12	0.88(2)
M4	0.5	0.83	0.17	0.99	0.01	1.00	0.00

Site	Equi-point fraction	Mn–WO Ca	Mn–WO Mn	Fe–WO Ca	Fe–WO Fe
M1	1.0	0.95	0.05(1)	0.97	0.03(1)
M2	1.0	0.97	0.03(1)	0.97	0.03(1)
M3	1.0	0.96	0.04	0.93	0.07

Site	Equi-point fraction	SRN Ca	SRN Mn	SCH Ca	SCH Mn
M1	1.0	0.34	0.66(1)	0.87	0.13(1)
M2	1.0	-0.02	1.02	0.36	0.64

*Obtained from least-squares refinement using a linear combination of Ca-Mn or Ca-Fe. Mn and Fe were grouped together and Mg effectively increases the apparent Ca occupancy. See text for discussion.
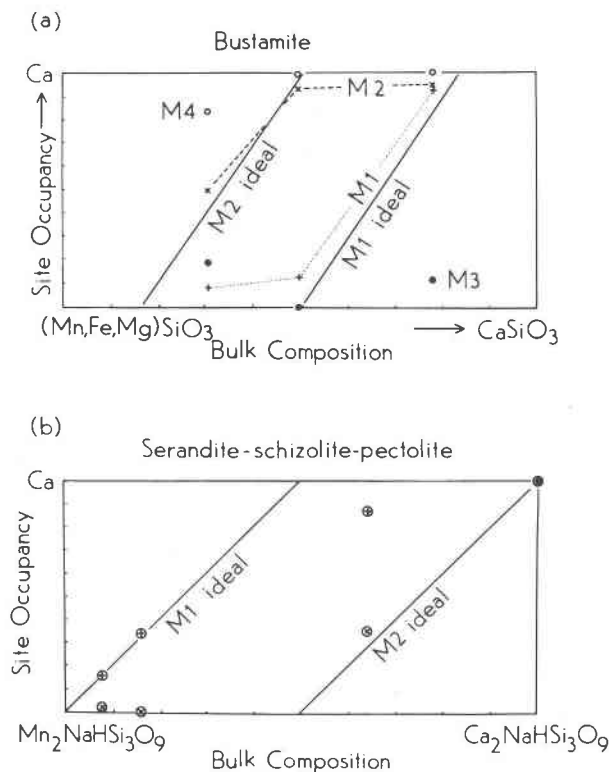
(a)

Bustamite

(b)

Serandite-schizolite-pectolite

Fig. 2. Variation of cation-site occupancies in (a) bustamite and (b) the pectolite–serandite series. The data on the most Mn-rich serandite are from Takéuchi et al. (1976b).

0.26 for specimen Mn–BS. The occupancy in $M1$ and $M2$ is variable, depending on the bulk composition of bustamite. On the subcalcic side of the 1:1 composition, $Ca(Mn,Fe,Mg)Si_2O_6$, $M2$ shows the most significant change in occupancy (Fig. 2a), whereas on the Ca-rich side $M1$ changes its cation occupancy.

In a recent review paper of pyroxenoid crystal chemistry, Takéuchi et al. (1976a) considered that substitution of Mn for Ca in the $M2$ site of bustamite would not exceed 50 percent. If so, specimen Mn–BS of this study, in which the occupancy of 49 percent Ca + 51 percent Mn was found in $M2$, would represent a theoretical limit to the Mn content of the bustamite structure. In natural bustamites the maximum $MnSiO_3$ component is approximately 2/3 in mole ratio, whereas the $CaSiO_3$ content can reach as high as 5/6 of the total.

The two wollastonite specimens studied contain approximately 4 mole percent $MnSiO_3$ or $FeSiO_3$. By analogy with the cation-ordering scheme in bustamite, the Mn and Fe atoms had been expected to show some ordering among the three cation sites in the wollastonite structure. The results, however, show that the Mn or Fe atoms are distributed over the three sites. The $M3$ site in Fe-wollastonite is slightly richer in iron, but there is little difference in occupancy for the other octahedral sites.

In the pectolite–schizolite–serandite series a stepwise substitution similar to that observed for bustamite is also found for the $M1$ and $M2$ sites (Fig. 2b). On the Ca-rich (pectolite) side of the (Ca:Mn = 1:1) composition, the $M1$ site is occupied by the larger Ca atom, whereas $M2$ is variable in its occupancy. Thus, for the 1:1 composition, ordering can be complete, as in one extreme case with 100 percent Ca in $M1$ and 100 percent Mn in $M2$. On the Mn-rich (serandite) side of the series, the occupancies of Ca and Mn in $M1$ change but $M2$ maintains its Mn occupancy. Thus, the Mn–Ca distribution in serandite is in complete agreement with that reported for a more Mn-rich serandite by Takéuchi et al. (1976b).

Interatomic distances

The octahedral cation–oxygen distances are also useful quantities in a discussion of cation occupancies of the site. The M–O distance, though not as quantitative as the occupancy refinement, can be used to differentiate two atoms that have similar X-ray scattering factors but different atomic size. For this purpose, the shortest M–O distance (or shortest two or three) would be a better parameter than the average of six or more M–O distances usually used. The longer M–O distance most likely results from other crystal structural factors, such as configuration of tetrahedra that share oxygen atoms at corners or edges with the octahedron, rather than from the larger size of the cation in the site.

In three bustamites studied, the $M1$–$OB1$ distances are, for example, 2.043, 2.042, and 2.225A (Table 7), clearly indicating that the third bustamite is different in its $M1$ occupancy from the first and the second, whereas the first bustamite is distinct in $M2$–$OA2$ (2.204, 2.289, and 2.284A, respectively). This result on M–O distances also suggests stepwise substitution in $M1$ and $M2$ of bustamite such as previously shown in Figure 2.

The relatively short $M3$–$OA2$ distance, about 2.15A in all three bustamites, would support the interpretation that the apparent Ca occupancy in $M3$ found in the occupancy refinement probably results from the existence in the site of Mg, which is much smaller in size than Ca. (Note also that the bulk $MgSiO_3$ concentration is higher in samples Mn–BS and Ca–BS, for which the apparent occupancy of Ca was indicated.)

In the pectolite–schizolite–serandite series, the

Table 7. M-O distances* (Å) for pyroxenoids

	Mn–BS	BS	Ca–BS		Mn–WO	Fe–WO		SRN	SCH
M1–OA1	2.149	2.170	2.302	M1–OA1	2.317	2.315	M1–OA1	2.381	2.451
–OA3	2.425	2.448	2.472	–OA3	2.546	2.544	–OA1	2.232	2.361
–OB1	2.043	2.042	2.225	–OB1	2.284	2.281	–OA2	2.313	2.399
–OB2	2.120	2.127	2.288	–OB2	2.256	2.246	–OA3	2.288	2.371
–OB3	2.293	2.293	2.404	–OB3	2.440	2.439	–OB1	2.240	2.336
–OC2	2.328	2.339	2.396	–OC3	2.416	2.414	–OB3	2.262	2.339
Mean	2.226	2.237	2.348	Mean	2.377	2.373	Mean	2.286	2.376
M2–OA2	2.204	2.289	2.284	M2–OA2	2.313	2.310	M2–OA1	2.364	2.355
–OA3	2.404	2.440	2.502	–OA3	2.496	2.495	–OA2	2.257	2.271
–OB1	2.229	2.293	2.270	–OB1	2.355	2.351	–OA2	2.252	2.308
–OB2	2.344	2.390	2.369	–OB2	2.305	2.309	–OA3	2.197	2.200
–OB3	2.473	2.520	2.444	–OB3	2.418	2.418	–OB2	2.169	2.240
–OC3	2.303	2.360	2.359	–OC2	2.405	2.402	–OB3	2.169	2.201
Mean	2.326	2.382	2.371	Mean	2.382	2.381	Mean	2.235	2.263
M3–OA1**	2.196	2.204	2.197	M3–OA1	2.336	2.327	A–OA3	2.270	2.295
–OA2	2.157	2.149	2.153	–OA1	2.415	2.408	–OB1	2.386	2.394
–OA3	2.183	2.203	2.234	–OA2	2.349	2.339	–OB2	2.502	2.557
				–OA2	2.430	2.426	–OC1	2.260	2.284
Mean	2.179	2.185	2.195	–OA3	2.412	2.401	–OC2	2.468	2.459
				–OB3	2.342	2.334	–OC2	2.713	2.758
M4–OA1**	2.438	2.443	2.457	–OC1	2.651	2.664	–OC3	2.518	2.622
–OA2	2.387	2.397	2.428				–OC3	2.922	3.077
–OB3	2.297	2.339	2.394	Mean	2.419	2.414			
–OC1	2.816	2.842	2.680						
							Mean, 6	2.401	2.435
Mean, 6	2.374	2.393	2.426				Mean, 8	2.505	2.556
8	2.485	2.505	2.490						

* Estimated standard errors: M–O = 0.001–0.003Å and A–O = 0.003–0.005Å
** Multiplicity of M3–O and M4–O for bustamite is 2.

changes in M–O distances are also consistent with the results of direct refinement of occupancies. When compared with values for serandite (Takéuchi et al., 1976b) and pectolite (Prewitt, 1967), $M1$–$OB1$, for example, increases (2.206, 2.240, 2.336, and 2.343Å) as the composition becomes more Ca-rich, showing a larger M–O change on the more Mn-rich side of the series. The $M2$–$OB3$, on the other hand, changes more on the Ca-rich side (2.153, 2.169, 2.201, and 2.321Å in sequence from serandite to pectolite), in agreement with its change in occupancy along the join (Fig. 2b).

Discussion

Stepwise substitution

The present study indicates that the cation substitution in the octahedral sites of bustamite and the pectolite–serandite series is a two-step process involving substitutions in the $M1$ and $M2$ sites. On the Ca-rich side of the solid solutions, the occupancy of $M1$ varies, whereas that of $M2$ is responsible for a change in chemistry on the Mn-rich side of the solid

solutions. This procedure can be considered in terms of the energy difference between ordered and anti-ordered states, i.e., $\{Ca(M2) + Mn(M1)\}$ vs. $\{Ca(M1) + Mn(M2)\}$. This energy difference must be so large that in a practical temperature range, disorder between $M1$ and $M2$ does not occur. Thus, the anti-ordered state in bustamite and the pectolite–serandite series resembles, to some extent, $\{Ca(M1) + Fe,Mg(M2)\}$ in clinopyroxenes, a state that is not observed (e.g. Ohashi et al., 1975a, for Ca–Fe clino-pyroxenes; Ohashi and Finger, 1976b, for Ca–Mg clinopyroxenes).

Crystal structures

The crystal structures of the three minerals studied are compared in Figure 3. Some structural features relevant to discussions of cation substitution are mentioned below. For more detailed structural comparisons, however, the readers are referred to Prewitt and Peacor (1964), Peacor and Prewitt (1963), and Prewitt and Buerger (1963).

The ratio of edges of the SiO_4 tetrahedron and the octahedron containing common divalent ions such as
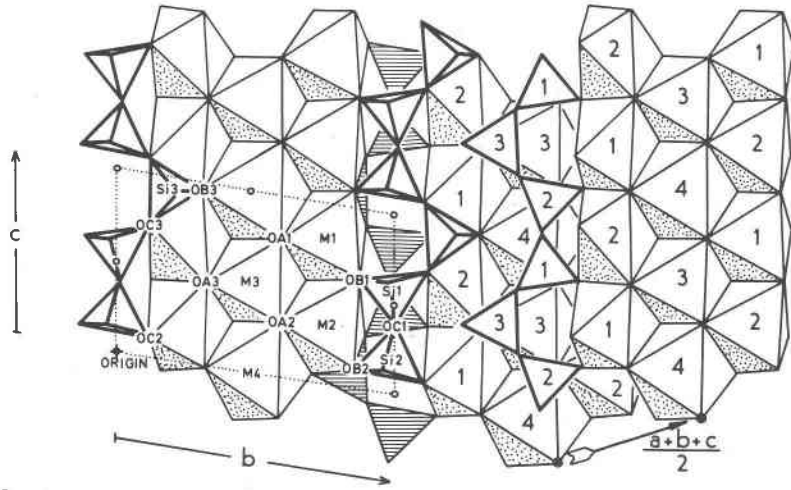
(a) Bustamite
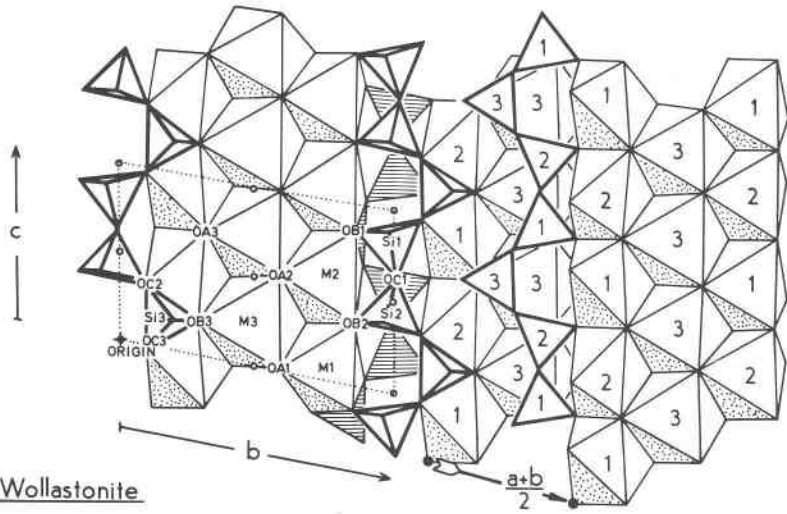
(b) Wollastonite
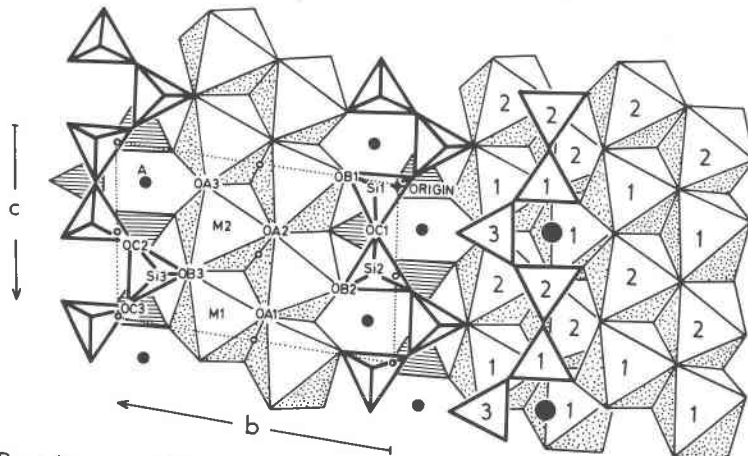
(c) Pectolite-serandite

Ca, Fe, or Mg is not in general either 1:1 or $\sqrt{3}$:2, the cases for which the ideal configurations of fully extended or fully rotated tetrahedral chains become possible in the pyroxene structure (Thompson, 1970; Papike *et al.*, 1973). The deviation from ideality requires the tetrahedra to rotate and tilt in order to fit the octahedral layers. The correlations between the octahedral cation size and tetrahedral rotation have been analyzed for pyroxenes (Papike *et al.*, 1973; Ohashi and Finger, 1974).

In cases involving the pyroxenoids, the rotation and tilting of the tetrahedra turn out to be even more important in controlling the octahedral size. A marked difference in behavior of cation substitution implies that changes in size and shape of each octahedron would affect the rest of the structure differently, particularly the tetrahedral layers.

Various arrangements of tetrahedra around a given octahedron have been discussed in a preliminary report of this study (Ohashi and Finger, 1976a). The following improved analyses of tetrahedral–octahedral linkages have been inspired by a recent discussion on the crystal chemistry of pyroxenoids by Takéuchi *et al.* (1976a), and Takéuchi and Koto (1977).

Apical oxygens of tetrahedra

The oxygen atoms in pyroxenoids are basically arranged in close-packed layers (Prewitt and Peacor, 1964) parallel to the (100) plane of the unit-cell setting used in this study. The structures projected on (100) are shown in Figure 3. If the three oxygens coordinated to a given silicon are in the same layer, they are called basal oxygens, and the fourth oxygen in the tetrahedron, denoted as an apical oxygen, is in the next oxygen layer.

The linkage of tetrahedra and octahedra at the apical oxygens of the tetrahedra is shown in Figure 4. A particularly important feature involves the two OA1–OA2 edges of octahedra, one connected to *adjacent* Si1 and Si2 tetrahedra, the other *across* Si3 (Fig. 4). Because the larger Ca atoms are present in pyroxenoids, the OA1–OA2 edge is much longer than the octahedral edges in pyroxenes (Takéuchi *et al.*, 1976a). Lengthening the OA1–OA2 distance causes considerable tilting of the basal faces of the tetra-

hedra out of the (100) plane of the new unit-cell setting. Thus, OC1 is shifted toward the octahedral face OA1–OA2–OB3 (Fig. 4a). The out-of-plane tilting does not exceed 7° of arc in pyroxenes (Ohashi and Finger, 1974, p. 525, Fig. 203), but reaches as much as 24° in specimen Ca–BS, resulting in a relatively short distance, 2.68A, for M4–OC1 (Table 7).

The out-of-plane tilting of tetrahedra affects the octahedra differently in the three minerals (Takéuchi *et al.*, 1976a). The coupling of tetrahedral tilting on the upper and lower sides of a given octahedron (Fig. 4a) is such that the two OA1–OA2 edges of one M site, say M4, expand, whereas those for another M site, say M3, are shortened in bustamite. The cation-occupancy refinements of bustamites indicate Mn in M3 and Ca in M4. Thus, an alternating arrangement of –Mn–Ca–Mn–Ca– in the central part of the octahedral strip is regarded as a key factor for the tetrahedral–octahedral linkage that leads to a structure of the bustamite type.

In contrast, changes of the tetrahedral tilting in the wollastonite structure (Fig. 4b) result in expansion of one OA1–OA2 edge but contraction of the OA1–OA2 edge on the other side of the octahedron. This fact probably explains why the size (thus the occupancy) of the M3 site in wollastonite can change very little from the Ca-occupied case. The band of –Ca–Ca–Ca–Ca– will constrain the wollastonite-type arrangement of tetrahedral and octahedral layers.

The linkage at the apical oxygens in the pectolite-serandite series (Fig. 4c) is different from that of either bustamite or wollastonite. Because one of the two OA1–OA2 edges does not directly affect the size of the octahedron, the constraint of the two tetrahedral layers on the size of sandwiched octahedra is less severe than in the above two minerals. Thus, the M1 and M2 octahedra in the pectolite–serandite series can change their size without changing the stacking topology of the adjacent tetrahedral layers. This analysis is consistent with the observed wide range of substitution in the M1 and M2 sites in pectolite-serandite.

Basal oxygens of tetrahedra

The tetrahedral–octahedral linkage at the basal oxygens is compared in Figure 5 for the hydrous and

Fig. 3. Portions of the structures of (a) bustamite, (b) wollastonite, and (c) pectolite, projected from $+a^*$ onto the plane parallel to the close-packed layers of oxygens. Atomic positions with full labels correspond to coordinates given in Table 5. Other cation sites are labeled only by the number *n* of Si*n* or M*n*. The diagram for pectolite has been turned upside down in the projection plane so that the tetrahedral chains have a similar orientation in the three minerals.
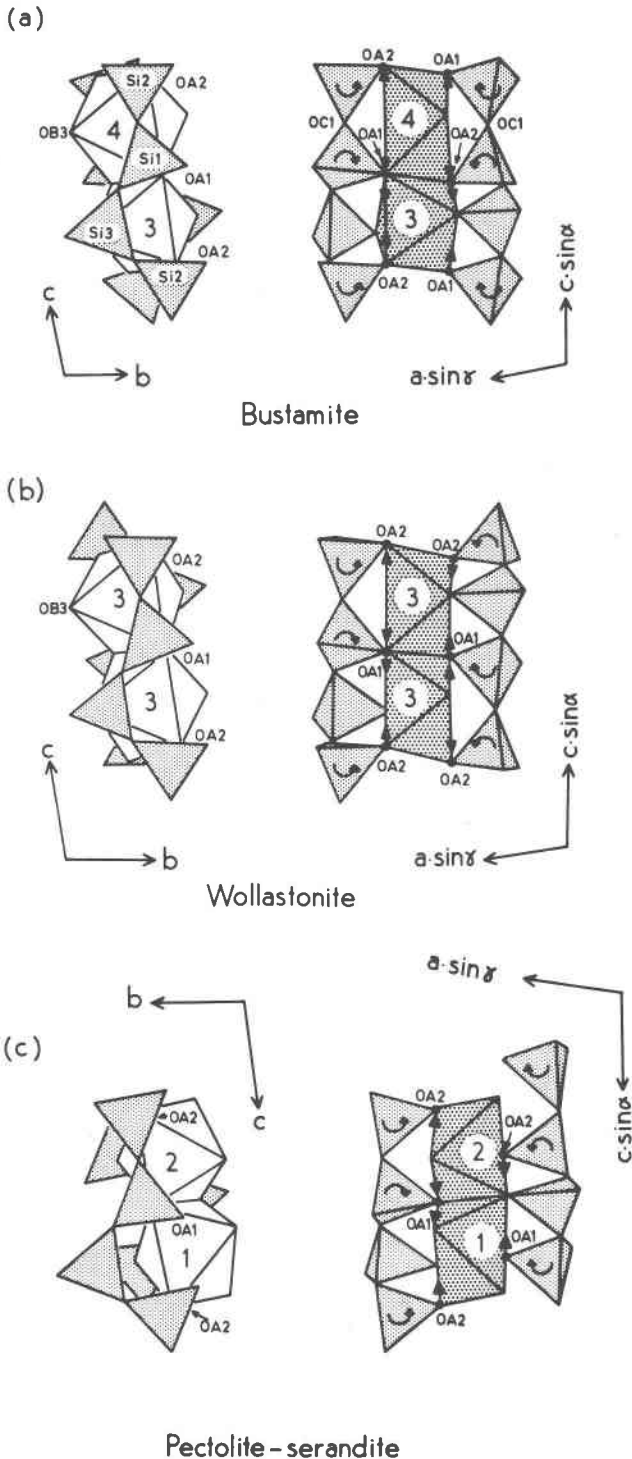
(a)

Bustamite

(b)

Wollastonite

(c)

Pectolite - serandite

Fig. 4. Tetrahedral–octahedral linkage at the apical oxygens of tetrahedra in (a) bustamite, (b) wollastonite, and (c) pectolite–serandite. Note that the tetrahedral tilting affects octahedral size differently in the three minerals.
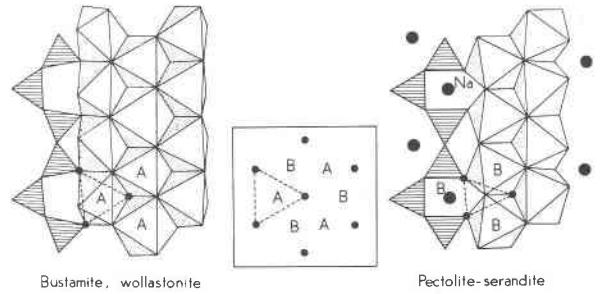

Bustamite, wollastonite   Pectolite-serandite

Fig. 5. Tetrahedral–octahedral linkage at the basal oxygens of tetrahedra in (a) bustamite and wollastonite, and (b) pectolite–serandite. The hatched tetrahedral chains shown are on a level lower than the octahedral layer. Triangular faces of octahedra in the two cases point to the opposite directions for the same orientation of the tetrahedral layer, corresponding to the two possible stacking schemes shown in the inset.

anhydrous pyroxenoids of this study. As shown in the inset of Figure 5, there are two possible ways to stack octahedral cations on a given layer of oxygens. Upper triangular faces of octahedra are pointing to the same direction as the basal face of the Si3 tetrahedron in wollastonite and bustamite. In pectolite–serandite, however, the triangular faces of the Si3 tetrahedron and octahedra point to opposite directions.

This difference in stacking holds also for pyroxenoids with a longer tetrahedral repeat, and is the characteristic distinction between the structures of the hydrous pyroxenoids (pectolite–serandite, babingtonite, and nambulite) and those of the anhydrous pyroxenoids (wollastonite, bustamite, rhodonite, and pyroxmangite). Recognizing two series of octahedral bands in pyroxenoid minerals, Takéuchi (1976) calls one the w–p series and the other p–p series, corresponding to anhydrous and hydrous pyroxenoids, respectively.

What makes two series of pyroxenoids? At first glance the Na atoms seem to determine the positions of the octahedral cations in pectolite. The tetrahedral *triplet* (Takéuchi *et al.*, 1976a)—a C-shaped cluster of three tetrahedra—provides a nearly square arrangement of oxygens that would be more suitable than a triangular arrangement for accommodating the larger alkali atoms. After the Na atoms are settled inside the C-shaped triplets, the two octahedra-wide bands must be in a position such as found in pectolite. In bustamite and wollastonite one octahedron is outside the open end of the C-shaped triplet, and other octahedra follow this configuration.

When alkali elements are found in hydrous pyroxenoids, they are in C-shaped triplets, *e.g.*, Na in pectolite (Prewitt, 1967) and Li and Na in nambulite, (Li,

Na)$Mn_4HSi_5O_{15}$ (Narita et al., 1975; Murakami et al., 1977). In babingtonite, $Ca_2Fe^{2+}Fe^{3+}HSi_5O_{15}$, however, the corresponding position is vacant (Araki and Zoltai, 1972); there must be an additional factor that determines the stacking sequence of tetrahedral–octahedral layers.

The fundamental difference between hydrous and anhydrous pyroxenoids is obviously the presence or absence of the hydrogen atoms. The position of hydrogen, however, has not been accurately determined; the proposed location of the H atom is between the two oxygen atoms, $OB1$ and $OB2$, at the opening of the C-shaped triplet (Prewitt, 1967; Araki and Zoltai, 1972). Because this hydrogen position yields a distance too short for Na–H, Takéuchi et al. (1976a,b) proposed, as a second possibility, a statistical distribution between two nearest $OB1$'s (or $OB2$'s) that are related by the inversion center. A method proposed by Donnay and Allmann (1970) indicates that the $OB1$, $OB2$, and $OB3$ oxygens are possible OH^- sites.

The role of hydrogen (or the O–H–O bridge if such a group exists) would be at least as important as that of the alkali atoms in making the structures of hydrous pyroxenoids distinct from those of anhydrous ones. Further studies are necessary to locate exactly the hydrogen atom and thus to delineate its role in the structure.

Compositional limits of bustamite

The $M1$ site in bustamite shows a complete substitution between Mn and Ca. Thus, the most Ca-rich bustamite corresponds ideally to the occupancy of $\{Ca(M1,M2,M4) + Mn(M3)\}$, resulting in a limiting composition of $Ca_{5/6}Mn_{1/6}SiO_3$ (the equipoint fraction is 0.5 for $M3$ and $M4$ and 1 for $M1$ and $M2$ in bustamite). The analogous composition $Ca_{5/6}Fe_{1/6}SiO_3$ was considered as a limiting composition for ferrobustamite (Rapoport and Burnham, 1972, 1973). From similar crystal-chemical considerations, Shimazaki and Yamanaka (1973) also predicted that the Ca concentration in their iron bustamite was the theoretical maximum. The cation-occupancy refinements of their Ca-rich iron bustamite (Y. Takéuchi, personal communication, 1976) and sample Ca–BS of this study have confirmed this ordering scheme.

The maximum Mn concentration in natural bustamite, however, is not $Ca_{1/6}Mn_{5/6}$, a reversed ratio of the maximum Ca limit, but approximately $Ca_{1/3}Mn_{2/3}$ (Mason, 1975; Hodgson, 1975). One of the most manganese-rich natural bustamites is sample Mn–BS of the present study. The refinement of this sample
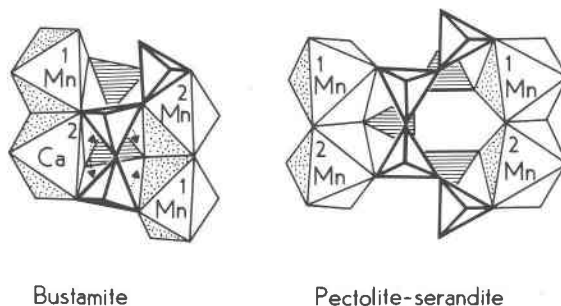

Bustamite   Pectolite–serandite

Fig. 6. Idealized Mn–Ca distribution in $M1$ and $M2$ for the most Mn-rich (a) bustamite and (b) pectolite–serandite. Short-range order of Mn–Ca in the two $M2$ sites connected by tetrahedra would explain the compositional limit of manganese bustamite (see text). In contrast, all four cation sites shown can be occupied by Mn in serandite.

suggests the idealized ordering of $\{Mn(M1,M3) + Ca(M4) + Ca_{1/2}Mn_{1/2}(M2)\}$. Takéuchi et al. (1976a) estimated that the maximum occupancy of Mn or Fe in $M2$ of bustamite would not exceed 50 percent, because one side of the $M2$ octahedron is linked to a pair of tetrahedra.

What is the controlling factor for limiting the occupancy of $M2$ to $Ca_{1/2}Mn_{1/2}$? One possible explanation is a short-range order of Mn and Ca between two adjacent $M2$ sites. Among several possibilities, the most likely $M2$ pair is the one connected by a pair of tetrahedra as shown in Figure 6a. If one $M2$ site is occupied by smaller cations such as Mn or Fe, the resultant rotation of the tetrahedra would require the other $M2$ site to remain large. In other words, the Mn–Mn combination in the above pair of $M2$'s is not allowed in this model, but combinations of Mn–Ca, Ca–Mn, and Ca–Ca can occur randomly in the structure. Thus, when averaged over the entire crystal, the Mn occupancy in $M2$ of bustamite cannot exceed 50 percent. In pectolite–serandite, however, the stacking is such that both $M1$ and $M2$ sites can be fully occupied by Mn (Fig. 6b).

Similar short-range order of cations might also be responsible for the compositional limits in other pyroxenoids, e.g., pyroxmangite and pyroxferroite. The composition of pyroxferroite is close to $Fe_6CaSi_7O_{21}$ (Chao et al., 1970), and the Ca concentration in pyroxmangite is less than 1/7 of the total octahedral cations (Momoi, 1964; Ohashi et al., 1975b). These facts would have been explained if all Ca were placed in one of the seven cation sites. Contrary to this prediction, Burnham (1971) has found that the Ca atoms are not restricted to one site. There must be other crystal-chemical explanations, such as a short-

Table 8. Characterization of cation sites in the octahedral layers of pyroxenoids

Site		Bustamite	Wollastonite	Pectolite-serandite
M1	Coordination	6	6	6
	Occupancy	Ca100 to (Mn,Fe)100	Ca100 to Ca95	Ca100 to Mn100
		Changes on Ca-rich side of solid solution		Changes on Ca-rich side of solid solution
M2	Coordination	6	6	6
	Occupancy	Ca100 to Ca50(Mn,Fe)50	Ca100 to Ca97	Ca100 to Mn100
		Changes on Mn-rich side of solid solution		Changes on Mn-rich side of solid solution
M3	Coordination	6	6 + 1*	
	Site symmetry	On inversion center		-------------------
	Occupancy	Essentially Mn or Fe	Ca100 to Ca93	
M4	Coordination	6 or 6 + 2*		
	Site symmetry	On inversion center	--------------------	-------------------
	Occupancy	Essentially Ca		
A	Coordination			8**
	Occupancy	-------------------	-------------------	Na

 * The seventh and eighth distances to OC depending on tetrahedral tilting (See Fig. 4).
** Including two longer distances to OC2 and OC3.

range order, for the compositional limit of $(Fe,Mn)_6CaSi_7O_{21}$ in pyroxferroite and pyroxmangite.

Conclusions

Cations in the octahedral layers play key roles in determining (1) the structure type and (2) the range of solid solutions in the pyroxenoid minerals. The roles of cations in the octahedral layers are summarized in Table 8 for the three pyroxenoid types of the present study.

If the occupancy of Ca and the smaller cations such as Mn, Fe, and Mg in a given site stays essentially invariant for a solid-solution series, the site is regarded as the *structure determinant*. The alternating distribution of Mn in $M3$ and Ca in $M4$, as –Mn–Ca–Mn–Ca–, is essential for the structure to be the bustamite type. When the corresponding sites are both occupied by Ca, forming the band of –Ca–Ca–Ca–Ca–, the structure must be the wollastonite type. In pectolite–serandite, the stacking of tetrahedral and octahedral layers is probably determined by the existence of the Na atoms. There is also a possibility that the structure determinant in hydrous pyroxenoids is the hydrogen atom, which has not been accurately located in the structure.

The wide range of solid solutions in bustamite and pectolite–serandite is achieved by the stepwise substitution of Ca and Mn (or Fe, Mg) in the $M1$ and $M2$ cation sites. On the Ca-rich side of the solid solution, mainly the occupancy of $M1$ changes, whereas $M2$ is variable in its occupancy on the subcalcic side of the solid solution. In addition to the stepwise substitution, another mechanism, such as a short-range order, is needed to explain the substitution limit of $Ca_{1/2}Mn_{1/2}$ in $M2$ of bustamite.

Note added in proof

The result of structural refinement of ferrobustamite from the Ofuku mine, Japan, has been recently published. Yamanaka, T., R. Sadanaga and Y. Takéuchi (1977) Structural variation in the ferrobustamite solid solution. *Am. Mineral., 62,* 1216–1224.

also extended to Mrs. M. L. Fanok for typing several versions of the text and extensive tables, to Miss D. M. Thomas for editing the manuscript, and to Mrs. L. Mager for typing the final manuscript.

References

Araki, T. and T. Zoltai (1972) Crystal structure of babingtonite. *Z. Kristallogr., 135*, 355–373.

Belov, N. V. (1961) *Crystal Chemistry of Large-Cation Silicates.* Consultants Bureau, New York.

Bøggild, O. B. (1903) On some minerals from the nepheline-syenite at Julianehaab, Greenland (erikite and schizolite). *Meddelelser om Grønland, 26,* 121–139.

Bragg, W. L., G. F. Claringbull and W. H. Taylor (1965) *Crystal Structures of Minerals.* Cornell University Press, Ithaca, New York.

Buerger, M. J. (1956) The determination of the crystal structure of pectolite, $Ca_2NaHSi_3O_9$. *Z. Kristallogr., 108,* 248–261.

——— and C. T. Prewitt (1961) The crystal structures of wollastonite and pectolite. *Proc. Natl. Acad. Sci., 47,* 1884–1888.

Burnham, C. W. (1966) Computation of absorption correction and the significance of end effect. *Am. Mineral., 51,* 159–167.

——— (1971) The crystal structure of pyroxferroite from Mare Tranquillitatis. *Proc. Second Lunar Sci. Conf., Geochim. Cosmochim. Acta, Suppl. 2,* 47–57.

Chao, E. C. T., J. A. Minkin, C. Frondel, C. Klein, Jr., J. C. Drake, L. Fuchs, B. Tani, J. V. Smith, A. T. Anderson, P. B. Moore, G. R. Zechman, Jr., R. J. Traill, A. G. Plant, J. A. Douglas and M. R. Dence (1970) Pyroxferroite, a new calcium-bearing iron silicate from Tranquillity Base. *Proc. Apollo 11 Lunar Sci. Conf.,* 65–79.

Cromer, D. T. (1965) Anomalous dispersion corrections computed from self-consistent field relativistic Dirac-Slater wave functions. *Acta Crystallogr., 18,* 17–23.

——— and J. B. Mann (1968) X-ray scattering factors computed from numerical Hartree-Fock wave functions. *Acta Crystallogr., A24,* 321–324.

Donnay, G. and R. Allmann (1970) How to recognize O^{2-}, OH^- and H_2O in crystal structures determined by X-rays. *Am. Mineral., 55,* 1003–1015.

Finger, L. W. (1969) Determination of cation distributions by least-squares refinement of single-crystal X-ray data. *Carnegie Inst. Wash. Year Book, 67,* 216–217.

———, C. G. Hadidiacos and Y. Ohashi (1973) A computer-automated, single-crystal X-ray diffractometer. *Carnegie Inst. Wash. Year Book, 72,* 694–699.

——— and E. Prince (1975) A system of FORTRAN IV computer programs for crystal structure computations. *U. S. Natl. Bur. Stand. Tech. Note, 854,* 133 p.

Hodgson, C. J. (1975) The geology and geological development of the Broken Hill Lode, in the New Broken Hill Consolidated Mine Australia, Part II: mineralogy. *J. Geol. Soc. Aust., 22,* 33–50.

Koto, K., N. Morimoto and H. Narita (1976) Crystallographic relationships of the pyroxenes and pyroxenoids. *J. Japan. Assoc. Mineral. Petrol. Econ. Geol., 71,* 248–254.

Lacroix, A. (1931) Les pegmatites de la synéite sodalitique de l'île Rouma (Archipel de Los, Guinée francaise). Descrition d'un nouveau minéral (sérandite) qu'elles renferment. *C. R. Acad. Sci. Paris, 192,* 187–194; abstracted in *Am. Mineral., 16,* 344 (1931).

Liebau, F. (1958) Über die Struktur des Schizoliths. *Neues Jahrb. Mineral. Monatsh.,* 227–229.

——— (1972) Silicon. Crystal chemistry. In K. H. Wedepohl, Ed., *Handbook of Geochemistry.* Springer-Verlag, Berlin.

Mamedov, K. S. and N. V. Belov (1956) Crystal structure of wollastonite. *Dokl. Akad. Nauk SSSR, 107,* 463–466.

Mason, B. (1973) Manganese silicate minerals from Broken Hill, New South Wales. *J. Geol. Soc. Aust., 20,* 394–404.

——— (1975) Compositional limits of wollastonite and bustamite. *Am. Mineral., 60,* 209–212.

Matsueda, H. (1973) Iron-wollastonite from the Sampo Mine showing properties distinct from those of wollastonite. *Mineral. J. (Japan), 7,* 180–201.

——— (1974) Immiscibility gap in the system $CaSiO_3$–$CaFeSi_2O_6$ at low temperatures. *Mineral. J. (Japan), 7,* 327–343.

Momoi, H. (1964) Mineralogical study of rhodonites in Japan with special reference to contact metamorphism. *Mem. Fac. Sci. Kyushu Univ. Ser. D. Geol., 15,* 39–63.

Morimoto, N. (1974) Problems on the crystal structures on pyroxenes. (in Japanese) *Chishitsugaku Ronshu,* No. 11, 303–321.

Muramaki, T., Y. Takéuchi and T. Tagai (1977) Lithium-hydro-rhodonite. *Acta Crystallogr., B33,* 919–921.

Nambu, M., K. Tanida and T. Kitamura (1970) Mineralogical study of manganese silicate ores in northeastern Japan. (VIII). Manganese wollastonite from Hijikuzu Mine. Iwate Prefecture. (in Japanese) *Bull. Res. Inst. Mineral. Dressing Metall., Tohoku Univ., 26,* 11–21.

Narita, H. (1973) *Crystal Chemistry of Pyroxene and Pyroxenoid Polymorphs of $MnSiO_3$.* Ph.D. Thesis, Osaka University, Osaka, Japan.

———, K. Koto and N. Morimoto (1975) The crystal structure of nambulite $(Li,Na)Mn_4Si_5O_{14}(OH)$. *Acta Crystallogr., B31,* 2422–2426.

Ohashi, Y. and L. W. Finger (1974) The effect of cation substitution on the symmetry and the tetrahedral chain configuration in pyroxenes. *Carnegie Inst. Wash. Year Book, 73,* 522–525.

——— and ——— (1976a) Stepwise cation ordering in bustamite and disordering in wollastonite. *Carnegie Inst. Wash. Year Book, 75,* 746–753.

——— and ——— (1976b) The effect of Ca substitution on the structure of clinoenstatite. *Carnegie Inst. Wash. Year Book, 75,* 743–746.

———, C. W. Burnham and L. W. Finger (1975a) The effect of Ca–Fe substitution on the clinopyroxene crystal structure. *Am. Mineral., 60,* 423–434.

———, A. Kato and S. Matsubara (1975b) Pyroxenoids: a variation in chemistry of natural rhodonite and pyroxmangite. *Carnegie Inst. Wash. Year Book, 74,* 561–564.

Papike, J. J., C. T. Prewitt, S. Sueno and M. Cameron (1973) Pyroxenes: comparisons of real and ideal structural topologies. *Z. Kristallogr., 138,* 254–273.

——— and M. Ross (1970) Gedrites: crystal structures and intra-crystalline cation distributions. *Am. Mineral., 55,* 1945–1972.

Peacor, D. R. and M. J. Buerger (1962) Determination and refinement of the crystal structure of bustamite, $CaMnSi_2O_6$. *Z. Kristallogr., 117,* 331–343.

——— and C. T. Prewitt (1963) Comparison of the crystal structures of bustamite and wollastonite. *Am. Mineral., 48,* 588–596.

Prewitt, C. T. (1967) Refinement of the structure of pectolite, $Ca_2NaHSi_3O_9$. *Z. Kristallogr., 125,* 298–316.

——— and M. J. Buerger (1963) Comparison of the crystal structures of wollastonite and pectolite. *Mineral. Soc. Am. Spec. Pap., 1,* 293–302.

—— and D. R. Peacor (1964) Crystal chemistry of the pyroxenes and pyroxenoids. *Am. Mineral.*, 49, 1527–1542.

Rapoport, P. A. and C. W. Burnham (1972) Structural chemistry of bustamite-type pyroxenoids on the wollastonite–hedenbergite join. *Geol. Soc. Am. Abstr. with Programs*, 7, 632–633.

—— and —— (1973) Ferrobustamite: the crystal structures of two Ca,Fe bustamite-type pyroxenoids. *Z. Kristallogr., 138*, 419–438.

Rutstein, M. S. (1971) Re-examination of the wollastonite–hedenbergite ($CaSiO_3$–$CaFeSi_2O_6$) equilibria. *Am. Mineral.*, 56, 2040–2052.

—— and W. B. White (1971) Vibration spectra of high-calcium pyroxenes and pyroxenoids. *Am. Mineral.*, 56, 877–887.

Schaller, W. T. (1955) The pectolite–schizolite–serandite series. *Am. Mineral.*, 40, 1022–1031.

Shimazaki, H. and T. Yamanaka (1973) Iron-wollastonite from skarns and its stability relation in the $CaSiO_3$–$CaFeSi_2O_6$ join. *Geochem. J. (Japan)*, 7, 67–79.

Sundius, N. (1931) On the triclinic manganifereous pyroxenes. *Am. Mineral., 16*, 411–429, 488–518.

Takéuchi, Y. (1976) Two structural series of pyroxenoids. *Proc. Japan Acad., 52*, 122–125.

——, K. Koto and T. Yamanaka (1976a) Crystal–chemical aspects of pyroxenoids. (in Japanese) *Japan. Assoc. Mineral. Petrol. Econ. Geol. Spec. Pap., 1*, 41–64.

——, Y. Kudoh and T. Yamanaka (1976b) Crystal chemistry of the serandite–pectolite series and related minerals. *Am. Mineral., 61*, 229–237.

—— and K. Koto (1977) A systematics of pyroxenoid structures. *Mineral. J. (Japan)*, 8, 272–285.

Thompson, J. B., Jr. (1970) Geometrical possibilities for amphibole structures: model biopyriboles. *Am. Mineral., 55*, 292–293.

Tilley, C. E. (1937) Wollastonite solid solutions from Scawt Hill, Co. Antrim. *Mineral. Mag., 24*, 569–572.

Veblen, D. and C. W. Burnham (1975) Triple-chain biopyriboles: newly discovered intermediate products of the retrograde anthophyllite–talc transformation, Chester, Vt. *Trans. Am. Geophys. Union, 56*, 1076.

—— and —— (1976) Biopyriboles from Chester, Vermont: the first mixed-chain silicates. *Geol. Soc. Am. Abstr. with Programs, 8*, 1153.

Zoltai, T. (1960) Classification of silicates and other minerals with tetrahedral structures. *Am. Mineral., 45*, 960–973.